Measurement and characterization of the three-dimensional coherence function in neutron interferometry

H. Rauch and H. Wölwitsch*
Atominstitut der Österreichischen Universitäten, A-1020 Wien, Austria

H. Kaiser, R. Clothier,† and S. A. Werner
Physics Department and Research Reactor Facility, University of Missouri—Columbia, Columbia, Missouri 65211
(Received 8 September 1995)

The spatial coherence function in all three orthogonal directions has been measured by means of perfect crystal neutron interferometry. It has been demonstrated that the coherence function is given by the Fourier transform of the related momentum distribution, which in turn is determined by the collimation and monochromatization of the beam incident upon and traversing the interferometer. Thus, a measurement of the coherence function can replace a measurement of the momentum distribution in certain cases. Retrieval of the coherence can be accomplished by phase echo and/or postselection methods. A complete retrieval of the coherence is impossible in principle due to unavoidable loss factors.

PACS number(s): 03.75.b, 03.65.Bz, 42.50.p

I. INTRODUCTION

During the past two decades, neutron interferometry has provided direct experimental realizations of many quantum Gedanken experiments [1–4]. Most of these experiments have been performed with perfect crystal interferometers where the strictly periodic arrangement of the atoms in a monolithic perfect silicon crystal provides a coherent beam splitting at twice the Bragg angle, a subsequent coherent deflection, and then a superposition at the exit plate of the interferometer. The phase difference between the coherent beams in this Mach-Zehnder interferometer can be affected by nuclear, electromagnetic, gravitational, or topological interactions, and an amplitude attenuation can be achieved by absorbing materials. Due to the very low phase-space density of existing neutron sources, neutron interferometry is a self-interference phenomena being observed nearly exclusively when only one neutron is inside the interferometer at a given time. In nearly all cases the next neutron does not yet exist as a free particle following fission of uranium in the reactor.

Coherence phenomena play an important role in any kind of interferometry [5–7]. Here we summarize some known results, add some additional ones, and analyze them in terms of general quantum optics, which can be applied to photon and matter waves as well. Indeed, neutrons have many well-known particle properties, but in interference experiments they behave like wave fields which provide the connection to the quantum optical terminology. In this connection, typical quantum optical phenomena like postselection and squeezing of Schrödinger-cat-like states [8], coherent photon exchange experiments [9,10], and experiments concerning counting statistics [11,12] have been reported in the literature. Coherence appears as a system property (neutron plus interferometer) which persists as long as it does not become destroyed by statistical or dissipative effects.

II. BASIC RELATIONS

The concept of coherence follows from the description of field properties by wave functions as they are used routinely in quantum physics and quantum optics [5–7]. Here we focus our attention on first-order coherence phenomena of Schrödinger quantum fields, which are described by

$$H\psi(\vec{r},t)=i\hbar\frac{\partial\psi(\vec{r},t)}{\partial t}. \tag{1}$$

The propagation of waves in free space from a source to a detector is described by a wave packet,

$$\psi(\vec{r},t)=\int a(\vec{k})e^{i(\vec{k}\cdot\vec{r}-\omega t)}d^3\vec{k}. \tag{2}$$

The amplitude factor $a(\vec{k})$ stems from creation $a_k^\dagger$ and annihilation a_k operators, which create or annihilate a mode with the corresponding $\vec{k}$ vector. The quantization steps of the coherent field between the source and the detector (a distance L apart) are extremely narrow ($\Delta k\sim 2\pi/L$) and, therefore, the integral form of the wave function can be used [6].

The first-order, two-point–two-time correlation function relating the physical situation at $(\vec{r},t)$ and $(\vec{r}',t')$ is given by

$$G^{(1)}(\vec{r},t;\vec{r}'t')=\mathrm{Tr}\{\rho\psi^*(\vec{r},t)\psi(\vec{r}',t')\}, \tag{3}$$

where

$$\rho=\int\psi^*(\vec{r},t)\psi(\vec{r},t)d^3\vec{r}dt=\int|a(\vec{k})|^2d^3\vec{k},$$

and $|a(\vec{k})|^2=g(k)$ is the density of states in $\vec{k}$ space. $G^{(1)}$ has the general features

*Present address: VÖEST-Alpine AG, A-4020 Linz, Austria

†Present address: Physics Department, Bethany College, Bethany, WV 26032.

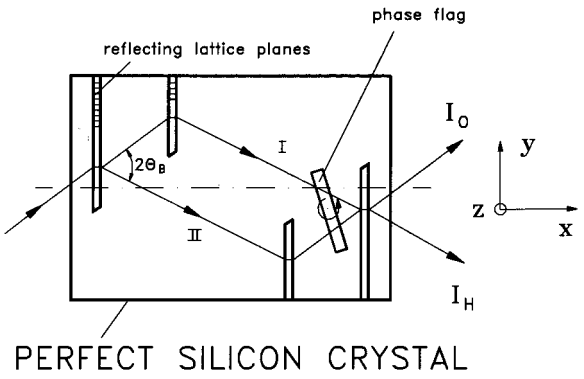

FIG. 1. Sketch of a skew symmetrically cut perfect crystal neutron interferometer. Rotating the phase flag changes the optical path lengths for path II relative to path I, thus generating an interferogram.

$$G^{(1)}(\vec{r},t;\vec{r},t)\geqslant 0 \tag{4a}$$

and

$$G^{(1)}(\vec{r},t;\vec{r},t)G^{(1)}(\vec{r}',t';\vec{r}',t')\geqslant|G^{(1)}(\vec{r},t;\vec{r}',t')|^2. \tag{4b}$$

These self-correlation functions can be measured by several interferometric methods where parts of the wave function can be spatially or temporally shifted compared to a reference beam. For neutron matter waves, this can be accomplished by perfect crystal interferometers where the wave function behind the interferometer is composed of a linear superposition of the wave functions originating from beam paths I and II (Fig. 1). In the case of an empty interferometer, these two contributions to the wave function in the forward direction (0) behind the interferometer are equal in amplitude and phase ($\psi_0^{\mathrm{I}}=\psi_0^{\mathrm{II}}$). This follows from symmetry considerations be cause they are transmitted-reflected-reflected (TRR) and reflected-reflected-transmitted (RRT), respectively. Thus,

$$\psi_0=\psi_0^{\mathrm{I}}+\psi_0^{\mathrm{II}}. \tag{5}$$

The related intensity can now be written as

$$I_0=\mathrm{Tr}\{\rho\psi_0^*(\vec{r},t)\psi_0(\vec{r},t)\}=G^{(1)}(\vec{r},t;\vec{r},t)+G^{(1)}(\vec{r}',t';\vec{r}',t') +2\,\mathrm{Re}G^{(1)}(\vec{r},t;\vec{r}',t'). \tag{6}$$

If we write the self-correlation function $G^{(1)}$ for $(\vec{r},t)\neq(\vec{r}',t')$ as a complex function,

$$G^{(1)}(\vec{r},t;\vec{r}',t')=|G^{(1)}(\vec{r},t;\vec{r}',t')|e^{i\chi(\vec{r},t;\vec{r}',t')}, \tag{7}$$

we then see that, in terms of the phase χ, the intensity is

$$I=G^{(1)}(\vec{r},t;\vec{r},t)+G^{(1)}(\vec{r}',t';\vec{r}',t') +2|G^{(1)}(\vec{r},t;\vec{r}',t')|\cos\chi(\vec{r},t;\vec{r}',t'). \tag{8}$$

One should note that $G^{(1)}(\vec{r},t;\vec{r},t)$ and $G^{(1)}(\vec{r}',t';\vec{r}',t')$ are the intensities originating from beam paths I and II, respectively.

The fringe visibility (contrast) of the interference pattern is related to the normalized correlation function $\Gamma^{(1)}(\vec{r},t;\vec{r}',t')$, that is,

$$\Gamma^{(1)}(\vec{r},t;\vec{r}',t')\equiv\frac{G^{(1)}(\vec{r},t;\vec{r}',t')}{[G^{(1)}(\vec{r};t;\vec{r},t)G^{(1)}(\vec{r}',t';\vec{r}',t')]^{1/2}}. \tag{9}$$

Combining Eqs. (2), (3), and (8), the complex degree of mutual coherence can be written as

$$\Gamma^{(1)}(\vec{r};t;\vec{r}',t')\propto\int|a(\vec{k})|^2e^{i[(\vec{r}-\vec{r}')\cdot\vec{k}-(t-t')\omega_k]}d^3\vec{k}\,d\omega_k. \tag{10}$$

This can be simplified by using the spatial and temporal translation invariances ($\vec{r}-\vec{r}'=\vec{\Delta}$, $t-t'=\tau$) and the free-space dispersion relation $\omega_k=\hbar k^2/2m$, such that

$$\Gamma^{(1)}(\vec{\Delta},\tau)=\int\rho(\vec{k},\omega)e^{i(\vec{k}\cdot\vec{\Delta}-\omega_k\tau)}d^3\vec{k}\;d\omega_k. \tag{11}$$

The Fourier transform given here is similar to the well-known van Hove formalism of neutron scattering [13]. We can now write the interference pattern (8) in the form

$$I(\vec{\Delta},\tau)=I_1+I_2+2\sqrt{I_1I_2}|\Gamma^{(1)}(\vec{\Delta},\tau)|\cos(\vec{k}\cdot\vec{\Delta}-\omega_k\tau), \tag{12}$$

and the visibility of the interference pattern

$$V=\frac{I_{\max}-I_{\min}}{I_{\max}+I_{\min}}=\frac{2\sqrt{I_1I_2}}{I_1+I_2}|\Gamma^{(1)}(\vec{\Delta},\tau)|. \tag{13}$$

For a completely coherent field $|\Gamma^{(1)}(\vec{\Delta},\tau)|=1$, whereas this function becomes zero for any $\vec{\Delta}\neq0$ and $\tau\neq0$ for a completely incoherent field. Any real experimental arrangement provides partially coherent fields where the coherence functions tend towards zero for $\vec{\Delta}\to\infty$ and $\tau\to\infty$. The coherence lengths $\vec{\Delta}_c$ and the coherence time τ_c are usually defined when the coherence function has decayed to a value $1/e$, but it should be mentioned that a damped oscillatory behavior occurs in certain cases. In such cases, the more general definition

$$\Delta_c^2=\frac{\int\Delta^2\Gamma^{(1)}(\Delta)\;d\Delta}{\int\Gamma^{(1)}(\Delta)\;d\Delta} \tag{14}$$

should be used [14].

Under conditions in which the temporal structure of the beam is slow, that is, quasistatic or even static, the corresponding time (τ) variations of $\Gamma^{(1)}(\vec{\Delta},\tau)$ can be separated from the spatial ($\vec{\Delta}$) correlations, such that $\Gamma^{(1)}$ may be written as a product $\Gamma^{(1)}(\vec{\Delta},0)\Gamma^{(1)}(0,\tau)$. For Gaussian momentum distributions having widths δk_i in each of the three orthogonal directions ($i=x,y,z$), one obtains a Gaussian coherence function

$$\Gamma(\vec{\Delta})=\prod_{i=x,y,z}e^{-[(\Delta_i\delta k_i)^2/2]}, \tag{15}$$

and $\Gamma(0,\tau)=1$ for all times. This is the case for continuous wave (cw) experiments. The coherence lengths Δ_i^c are directly related to δk_i by the uncertainty relations

$$\Delta_i^c \delta k_i = \tfrac{1}{2}. \tag{16}$$

Since we are only concerned with first-order coherence here, we have suppressed the superscript (1) on the coherence function in Eq. (15).

III. COHERENCE MEASUREMENTS

In neutron interferometry a spatial shift between the two coherent beams can be provided by a phase-shifting slab which changes the optical path length according to its index of refraction n and its thickness D_0. The boundary condition of quantum mechanics requiring continuity of the wave function allows only the normal $(\hat{\vec{s}})$ component of the momentum to change at the slab surface, resulting in a spatial shift of the wave packet [15,16]:

$$\vec{\Delta} = (1-n)\hat{\vec{s}}\, D_0, \tag{17}$$

which is related to the phase shift

$$\chi = (n-1)kD_{\text{eff}} = -Nb_c\lambda D_{\text{eff}} = \vec{\Delta}\cdot\vec{k}. \tag{18}$$

Here N and b_c are the atom density and the coherent scattering length of the phase shifter material, and $D_{\text{eff}}=D_0/(\hat{\vec{k}}\cdot\hat{\vec{s}})$ represents the neutron path length inside the material slab. Absorption (σ_a), incoherent scattering (σ_{incoh}), and small-angle scattering (σ_{SAS}) processes which can be described by an imaginary term in the index of refraction cause a loss of intensity of the beam reflected into the detector. Variations of the thickness (δD) and of the density (δN) of the phase shifter across the beam cross section cause a variance of the phase shift, and also several unavoidable imperfections of the interferometer crystal itself and residual vibrations cause $|\Gamma(0,0)|$ to be less than unity, which leads to an incomplete modulation of the beam. Thus, the observed interference pattern has the general form

$$I(\vec{\Delta}) = I_0[A + B\cos(\vec{\Delta}\cdot\vec{k}+\varphi_0)], \tag{19}$$

where I_0A and I_0B corresponds to I_1+I_2 and to $2\sqrt{I_1I_2}|\Gamma(\vec{\Delta})|$ of Eq. (12). The attenuation processes cause a reduction of the intensity in beam path II, i.e., [17],

$$I_{\text{II}}'(D_0) = I_{\text{II}}(0)\exp[-N\sigma_t D_{\text{eff}}], \tag{20}$$

with $\sigma_t=\sigma_a+\sigma_{\text{incoh}}+\sigma_{\text{SAS}}$. For very strong beam attenuations, additional (fluctuation) effects come into play [18]. The fluctuation processes do not depend on the overall thickness (or density) of the phase shifter and result in additional damping factors to the coherence function [19,20]; thus the experimentally measured coherence function is

$$|\Gamma(\vec{\Delta})|_{\text{exp}} = \exp\left\{-\left[\left(\frac{\delta D}{D_0}\right)^2+\left(\frac{\delta N}{N_0}\right)^2\right]\times(\vec{\Delta}_0\vec{k}_0)^2 \Big/ 2\right\}|\Gamma(\vec{\Delta})|. \tag{21}$$

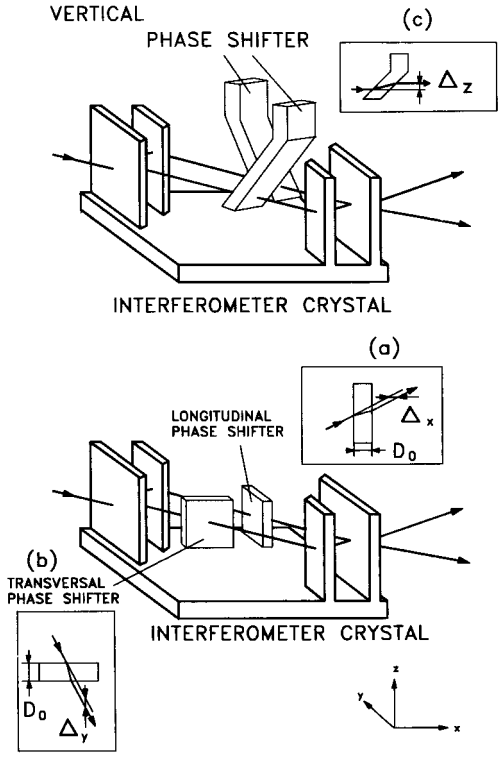

FIG. 2. Phase-shifting slab arrangements for the measurements of the longitudinal (a), transverse (b), and vertical (c) coherence function.

All parameters entering Eq. (19) can be measured separately. When no phase shifter is inserted (perfect phase flag only), one measures $|\Gamma(0)|$ and ϕ_0; and when the beams are alternately closed off, one measures I_{I} and I_{II} for different thicknesses of the phase shifter. Because we are mostly interested in the coherence function, one defines the normalized degree of coherence

$$\gamma(\vec{\Delta},\tau) = \frac{|\Gamma(\vec{\Delta},\tau)|}{|\Gamma(0,0)|}, \tag{22}$$

which is the function to be compared with theory.

The above formulas show that spatial coherence is a three-dimensional phenomena. Figure 2 shows how wave-packet displacements in three mutually perpendicular directions can be experimentally realized within a perfect crystal interferometer. The resulting degree of coherence (contrast) is measured when an additional thin auxiliary phase flag is rotated around a vertical axis in the first gap of the interferometer.

A. Longitudinal coherence, x direction

In this case, the surface of the phase shifter is perpendicular to the reflecting lattice planes of the Si-crystal interferometer which shifts the wave packet in a direction where the perfect crystal does not influence the original momentum distribution function. The related spatial shift of the wave packets [see Fig. 2(a)] becomes

$$\Delta_x = -Nb_c\lambda^2 D_0/2\pi, \tag{23}$$

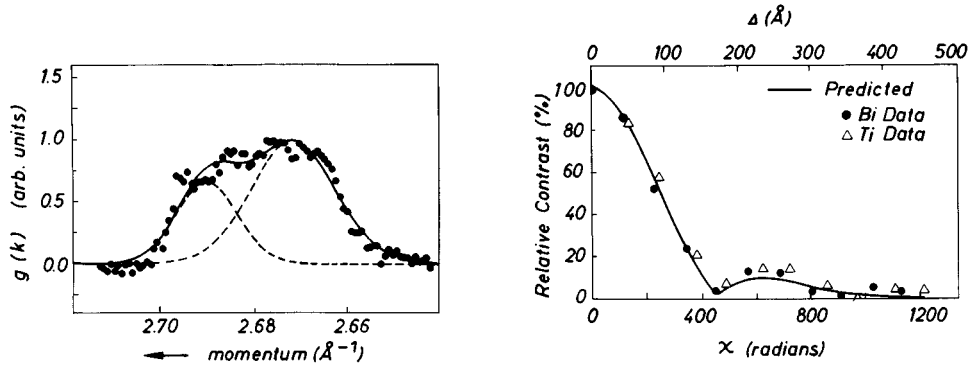

FIG. 3. Measured momentum distribution $g(k)$ (left) and coherence function (right) in the longitudinal direction [23].

and the corresponding phase shift is

$$\chi=\vec{\Delta}\cdot\vec{k}=-Nb_c\lambda D_0/\cos\varphi_B, \tag{24}$$

where ϕ_B denotes the Bragg angle. Related experiments have been carried out since the beginning of neutron interferometry [21–23]. They have shown a more or less continuous reduction of the fringe visibility at high order which results from the smooth bell-shaped momentum distribution in that direction. Figure 3 shows the result of a more recent experiment carried out at the MURR Reactor, where the momentum (wavelength) distribution had a non-Gaussian shape as it was determined by rocking an additional silicon analyzer crystal in the dispersive position through the I_0 beam shown in Fig. 1 [23,24]. The full lines are the mutual Fourier transforms as it is expected from Eq. (11).

B. Transverse coherence, *y* direction

In this case, the surface of the phase shifter is parallel to the reflecting lattice planes where the momentum distribution becomes strongly influenced due to the dynamical diffraction effects from the perfect crystal [25]. The resulting momentum distribution becomes rather narrow ($\Delta k_y/k_0\cong 10^{-5}$), exhibiting an oscillatory structure. The related spatial shift of the wave packet [see Fig. 2(b)] becomes

$$\Delta_y=-Nb_c\lambda^2 D_0/2\pi \tag{25}$$

and the phase shift reads as

$$\chi=-2Nb_c D_0 d, \tag{26}$$

where the Bragg relation $\lambda=2d\sin\Theta_B$ has been used with the Si interferometer lattice plane spacing d. This phase shift behaves nondispersively up to rather high interference orders and, therefore, the visibility of the interference fringes are correspondingly enhanced compared to the case of a longitudinal phase shifter. Related experiments have been performed at the ILL reactor and have verified this behavior [26]; see Fig. 4. The contrast is shown around the 250th interference order when the path length of the neutron beam inside the phase shifter is 33.8 mm and an auxiliary thin Al phase shifter is rotated inside the interferometer. The reduction of the contrast in the dispersive (longitudinal) x direction is caused mainly by the effect of the coherence function $|\Gamma(\vec{\Delta})|$ and not by beam attenuation and phase-shift fluctuations [Eqs. (20) and (21)]. The reduction of the contrast in the nondispersive (transverse) y-direction case is caused nearly exclusively by beam attenuation and phase-shift fluctuation effects and only very little by the coherence function. The coherence function for the nondispersive position has been calculated within the framework of spherical-diffraction theory where the contrast of a defocused interferometer is evaluated [27–29]. An interpretation in terms of a mutual coherence function has been given by Holy [30] and Petrascheck [15,16]. There is a nonvanishing contrast over the whole width of the Borrmann fan as shown in Fig. 5. The plotted results are for a thickness of the perfect crystal $D_{\rm cryst}$, which is 10 times the characteristic length $\Lambda=(2db_cN)^{-1}$, which amounts to about 10 μm for most silicon reflections. The coherence length has to be extracted by using Eq. (13) and some influence of the coherence function appears only beyond the $\sim 10^4$ interference order, i.e., at thicknesses where all other damping factors usually dominate.

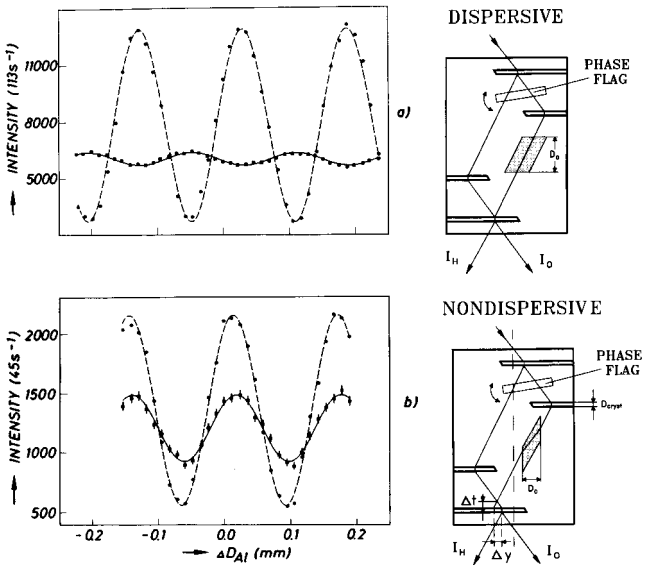

FIG. 4. Measured interference pattern around the 250th interference order for phase shifts in the longitudinal (a) and the transverse (b) direction [26]. (The dashed lines represent the interference pattern around zero interference order.) The transverse coherence length Δ_y^c is related to the defocusing distance Δt by $\Delta_y^e=2\Delta t\,\tan\theta_B$.

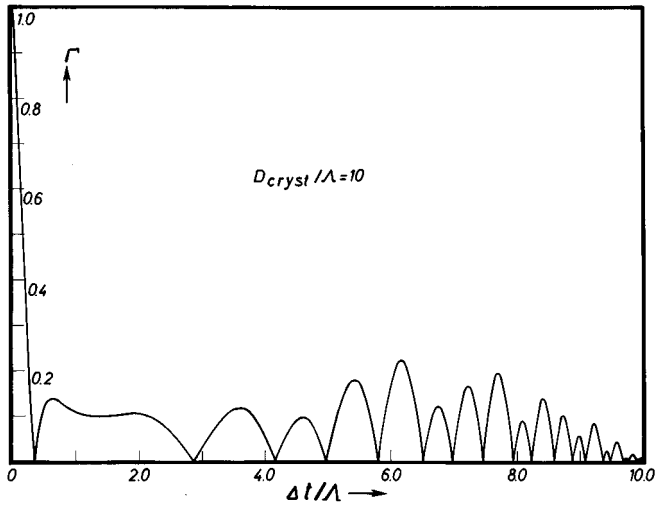

FIG. 5. Calculated coherence function in the transverse direction [16], plotted here as a function of the defocusing distance Δt (see Fig. 4).

C. Vertical coherence, *z* direction

In this case, a vertical shift Δ_z of the trajectories is achieved by a phase-shifting slab whose surface is tilted with respect to the horizontal plane by an angle φ, as shown in Fig. 2(c). This small spatial shift, due to refraction in the tilted slab, is given by

$$\Delta_z = -\tan\varphi \frac{\lambda^2 N b_c}{2\pi} D_0, \tag{27}$$

and the corresponding total phase shift becomes

$$\chi = -N b_c \lambda D_0 / \cos\varphi. \tag{28}$$

Such a phase shifter produces phase shifts in other directions, too, which have to be balanced by a proper phase shifter put into the reference beam and which compensates for beam attenuation as well.

Experiments using phase shifters with different thicknesses and tilt angles were performed at the MURR reactor (Fig. 6). At this interferometer setup, a twin focusing monochromator made up of pyrolytic graphite (PG) crystals (Fig. 6) was used, which produced a double-humped momentum distribution in the vertical direction as it was measured by scanning a horizontal slit (1 mm) through the intensity distribution behind a static slit (1 mm) placed at the interferometer table. These measurements were performed at different beam heights and averaged afterwards. The contrast was extracted from interferograms obtained by rotating an auxiliary phase shifter around a vertical axis with various tilted phase shifters and compensator phase-shifter slabs inserted into the two beams of the interferometer. This contrast (fringe visibility) directly yields the coherence function as it is plotted in Fig. 6. The full lines in Figs. 6(c) and 6(d) correspond to an optimal fit to the data and they are related to each other by their mutual Fourier transformations.

IV. DISCUSSION

The results show that spatial coherence is a basic three-dimensional phenomenon, and that related coherence functions can be obtained from the contrast of the interference pattern when variously oriented phase-shifting slabs are inserted into the interferometer. The coherence function in a certain direction is the Fourier transform of the related momentum distribution in that direction. Thus, it is determined by the collimation and monochromatization defining the beam. In this respect, the coherence function represents beam properties rather than single particle properties. Nevertheless, within quantum mechanics, the related wave function [Eq.

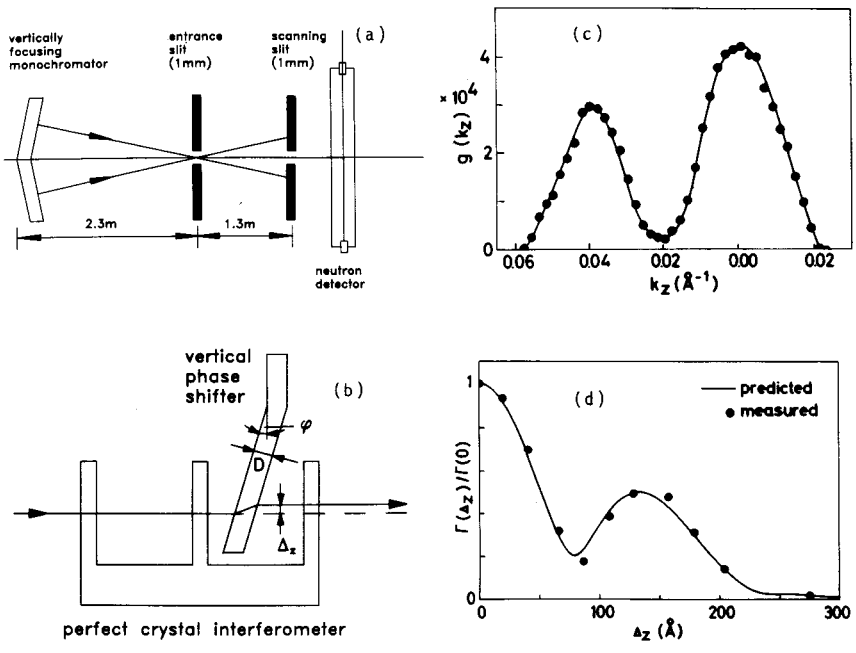

FIG. 6. (a) Diagram showing the twin focusing PG monochromator at beam port *C* at MURR. (b) Diagram showing the tilted phase shifters in the interferometer used to determine the vertical (*z*) coherence function. (c) Measured momentum distribution and (d) measured coherence function in the vertical direction.

(2)] can also be attributed to a single neutron, but this quantum system should also always be connected to a certain beam. That is, the wave function contains at the same time properties of the quantum system and of the apparatus as well, which can be seen as a basic feature of quantum mechanics.

The coherence experiments described in this article have been performed with perfect crystal interferometers. For representative usual values for the collimation and monochromatization, the measured coherence length in the longitudinal direction is about 100 Å, in the transverse direction about 50 000 Å, and in the vertical direction about 50 Å. These values define the phase-space volume and from the measured intensity the related phase-space density (a dimensionless quantity) of about 10^{-14} neutrons can be extracted, which corresponds to the expected phase-space density behind a thermal moderator of a standard neutron source. The size of the coherence packet in some sense describes the volume which the neutron ''sees'' when it interacts with its environment. This has been elucidated in an experiment where the wave packet was sent through an absorbing lattice which was oriented in various ways in relation to the three axes of the packet [31].

The question may arise, whether the coherence vanishes when the coherence function becomes zero at large phase shifts. Several recent postselection experiments for neutrons and electrons [8,22–24,32] have shown that this is not the case and that interference fringes and coherence phenomena can be revived when a proper position, momentum, or time selection is applied to the beam, even subsequent to superposition of the two coherent beams in the last crystal of the neutron interferometer. In the case of large spatial separations of the interfering packets ($\Delta \gg \Delta^c$), when $|\Gamma(\Delta)|$ becomes zero and the interference fringes disappear, the coherence phenomena manifest themself in momentum space by an intrinsic modulation of the momentum distribution [33]. This indicates that coherence cannot be destroyed by any Hamiltonian interaction but only by stochastic and dissipative effects [34–36]. Such effects become more influential the larger the spatial separation of the (potentially) interfering wave packets, which thereby provides a natural limit on how far so-called coherent Schrödinger-cat-like states can be separated. The interaction with the environment, phase shifter, or detector must not be of purely statistical nature, but one that can cause a quantum entanglement between the system and the detector. The random-average model of coherence loss provides in this case a proper description of the loss of coherence [20,37,38].

Only spatial-coherence phenomena have been treated in this paper, but it should be mentioned that temporal-coherence properties can also be elucidated by neutron interferometry. In this case, energy is exchanged differently in both beams than can be achieved by applying a Zeeman energy exchange between the neutron and a resonator coil [9] or by multiphoton exchange in an oscillating field [10].

ACKNOWLEDGMENTS

This work was supported by the Fonds zur Förderung der Wissenschaftlichen Forschung in Austria (Project No. P8456) and by the Physics Division of the NSF (Grant Nos. PHY-9024608 and INT-8712122).

[1] *Neutron Interferometry*, edited by U. Bonse and H. Rauch (Clarendon, Oxford, 1979).
[2] S. A. Werner and A. G. Klein, *Methods of Experimental Physics* (Academic, New York, 1986), Vol. 23, Part A, Chap. 4, p. 259.
[3] *Matter Wave Interferometry*, edited by G. Badurek, H. Rauch, and A. Zeilinger (North Holland, Amsterdam, 1988).
[4] S. A. Werner, Class. Quantum Grav. **11**, A207 (1994).
[5] M. Born and E. Wolf, *Principles of Optics* (Pergamon, Oxford, 1980).
[6] D. F. Walls and G. J. Milburn, *Quantum Optics* (Springer Verlag, Berlin, 1994).
[7] W. Lauterborn, T. Kurz, and M. Wiesenfeldt, *Coherent Optics* (Springer Verlag, Berlin, 1995).
[8] D. J. Jacobson, S. A. Werner, and H. Rauch, Phys. Rev. A **49**, 3196 (1994).
[9] G. Badurek, H. Rauch, and D. Tuppinger, Phys. Rev. A **34**, 2600 (1986).
[10] J. Summhammer, K. A. Hamacher, H. Kaiser, H. Weinfurter, D. L. Jacobson, and S. A. Werner, Phys. Rev. Lett. **75**, 3206 (1995).
[11] H. Rauch, J. Summhammer, M. Zawisky, and E. Jericha, Phys. Rev. A **42**, 3726 (1990).
[12] M. Zawisky, H. Rauch, and Y. Hasegawa, Phys. Rev. A **50**, 5000 (1994).
[13] L. van Hove, Phys. Rev. **95**, 249 (1954).
[14] J. Perina, *Coherence of Light* (Van Nostrand, London, 1973).
[15] D. Petrascheck, Phys. Rev. B **35**, 6549 (1987).
[16] D. Petrascheck, Physica B **151**, 171 (1988).
[17] J. Summhammer, H. Rauch, and D. Tuppinger, Phys. Rev. A **36**, 4447 (1987).
[18] M. Namiki, S. Pascazio, and H. Rauch, Phys. Lett. A **173**, 87 (1993).
[19] H. Rauch and M. Suda, Phys. Status Solidi A **25**, 495 (1974).
[20] A. Stern, Y. Aharonov, and Y. Imry, Phys. Rev. A **41**, 3436 (1990).
[21] H. Rauch, in *Neutron Interferometry* ([1]), p. 161.
[22] H. Kaiser, S. A. Werner, and E. A. George, Phys. Rev. Lett. **50**, 560 (1983).
[23] R. Clothier, H. Kaiser, S. A. Werner, H. Rauch, and H. Wölwitsch, Phys. Rev. A **44**, 5357 (1991).
[24] H. Kaiser, R. Clothier, S. A. Werner, H. Rauch, and H. Wölwitsch, Phys. Rev. A **45**, 31 (1992).
[25] H. Rauch and D. Petrascheck, in *Neutron Diffraction*, edited by H. Dachs, Topics in Current Physics Vol. 6 (Springer, Berlin, 1978), p. 303.
[26] H. Rauch, E. Seidl, D. Tuppinger, D. Petrascheck, and R. Scherm, Z. Phys. B **69**, 313 (1987).
[27] U. Bonse and E. te Kaat, Z. Phys. **14**, 243 (1971).
[28] D. Petrascheck and R. Folk, Phys. Status Solidi A **36**, 147 (1976).

[29] W. Bauspiess, U. Bonse, and W. Graeff, J. Appl. Cryst. **9**, 68 (1976).
[30] V. Holy, Phys. Status Solidi B **101**, 575 (1980).
[31] H. Rauch and J. Summhammer, Phys. Rev. A **46**, 7284 (1992).
[32] M. Nicklaus and F. Hasselbach, Phys. Rev. A **48**, 152 (1993).
[33] H. Rauch, Phys. Lett. A **173**, 240 (1993).
[34] D. F. Walls and G. J. Milburn, Phys. Rev. A **31**, 2403 (1985).
[35] W. Schleich, M. Pernigo, and Fam Le Kien, Phys. Rev. A **44**, 2172 (1991).
[36] H. Rauch and M. Suda, Appl. Phys. B **60**, 181 (1995).
[37] W. Wooters and W. Zurek, Phys. Rev. D **19**, 473 (1979).
[38] S. M. Tan and D. F. Walls, Phys. Rev. A **47**, 4663 (1993).